

RSC Advances



This is an *Accepted Manuscript*, which has been through the Royal Society of Chemistry peer review process and has been accepted for publication.

Accepted Manuscripts are published online shortly after acceptance, before technical editing, formatting and proof reading. Using this free service, authors can make their results available to the community, in citable form, before we publish the edited article. This *Accepted Manuscript* will be replaced by the edited, formatted and paginated article as soon as this is available.

You can find more information about *Accepted Manuscripts* in the [Information for Authors](#).

Please note that technical editing may introduce minor changes to the text and/or graphics, which may alter content. The journal's standard [Terms & Conditions](#) and the [Ethical guidelines](#) still apply. In no event shall the Royal Society of Chemistry be held responsible for any errors or omissions in this *Accepted Manuscript* or any consequences arising from the use of any information it contains.

**Formation of Cathode Buffer Layer by Surface Segregation of Fluoroalkyl
Modified ZnO for Polymer Solar Cells**

Licheng Tan^{1,2}, Zhijuan He¹, Yiwang Chen^{*1,2}

¹School of Materials Science and Engineering/Institute of Polymers, Nanchang University, 999 Xuefu Avenue, Nanchang 330031, China; ²Jiangxi Provincial Key Laboratory of New Energy Chemistry, College of Chemistry, Nanchang University, 999 Xuefu Avenue, Nanchang 330031, China

Abstract

Novel zinc oxide nanoparticles (ZnO NPs) modified by silanization using triethoxy-1H,1H,2H,2H-tridecafluoro-n-octylsilane (TTFO), referred as ZnOF NPs, have been successfully synthesized. Driven by the surface segregation behavior of the fluoroalkyl chains ascribed to their low surface energy, ZnOF NPs can migrate from the blend system with poly(3-hexylthiophene):[6,6]-phenyl-C₆₁-butyric acid methyl ester (P3HT:PCBM) to the surface of active layer during annealing process and consequently self-assemble as a cathode buffer layer. The addition of functionalized ZnOF NPs assists the stacking of P3HT chains to form favorable morphology of active layer with remarkable phase separation, especially upon annealing optimization in o-DCB solvent. The best power conversion efficiency (PCE) of 2.4% is achieved with open-circuit voltage (V_{oc}) of 0.49 V, short-circuit current density (J_{sc}) of 8.1 mA/cm² and fill factor (FF) of 61%, based on the self-assembly cathode buffer layer of ZnOF NPs (5 wt.%) upon annealing in o-DCB. Therefore, this novel approach could realize fabricating both active layer and cathode buffer layer through a single step, which not only simplifies the fabrication procedure and reduces the manufacturing cost of the polymer solar cells, but also increases PCE by reduction of

* Corresponding author. Tel.: +86 791 83968703; fax: +86 791 83969561. *E-mail address*: ywchen@ncu.edu.cn (Y. Chen).

a Schottky barrier at the interface and the stability of the devices.

Keywords: self-assembly; zinc oxide; fluoroalkyl; cathode buffer layer

Introduction

Organic photovoltaic devices (OPVs) based on conjugated polymer materials have been paid a tremendous amount of attention, partly because they feature many advantageous properties, including light weight, mechanical flexibility, low-temperature and low-cost fabrication of large-area devices [1-3]. Recently, increasing research efforts have been devoted to enhancing the photovoltaic efficiency. Optimization the morphology of the active layer by improving the processing methods or adding some additives in the active layer, as well as utilizing an effective buffer interface (including hole and electron transporting layer) are valid for realizing a high efficiency, since they affect the flow of charge carriers across or along material interfaces largely [4-10].

The buffer interface has been commonly employed to improve the contact between the active organic layer and electrodes. Lithium fluoride (LiF) [11], cesium carbonate (Cs_2CO_3) [12], titanium oxide (TiO_x) [13], zinc oxide (ZnO) [14] and self-assembled monolayer [15] are used as n-type electron transporting layer materials in polymer solar cells. They create an effective metal-organic interface, which decreases the contact resistance between the active layer and cathode electrode, forms a favorable dipole moment across the junction and makes the Fermi levels of layers matching well to enhance the efficiency of charge collection [8]. The buffer layer also prevents oxygen and humidity diffusing into the active layer, thereby improving the lifetime of the unpackaged devices.

Generally speaking, the formation of the conventional cathode buffer layer (CBL) needs an additional fabrication step. For instance, LiF is prepared through vacuum

deposition [11,15-17], ZnO or TiO_x is dipped or spin coated [13,14,18-20]. The additional processes have adverse effect on the active layer, make the craft complicated and improve the manufacture cost to some extent. Furthermore, owing to the vertical phase separation with instability in thermodynamic, the elements of the additional buffer layer may diffuse into the active layer [5], which could affect the efficiency and the stability of the solar cells. Hence, to fabricate both organic materials and cathode buffer layer by a single step and keep the materials stable in a long time are valuable. *Zhang* et al. reported the application of non-conjugated polymers (surfactant), such as poly(ethylene oxide) (PEO), as the buffer layer between the active layer and the metal cathode to improve the polymer devices performance [21]. *Cheun* et al. studied the role of thermally-induced vertical phase segregation and crystallization on the photovoltaic performance of bulk heterojunction inverted polymer solar cells [22]. *Clark* et al. found that there was a slightly [6,6]-phenyl-C₆₁-butyric acid methyl ester (PCBM)-rich layer between the active layer and the air interface during the film casting. Furthermore, the phenomenon of spontaneous vertical phase separation in polymer photovoltaic devices decided by the different free energy had been verified by angle-resolved X-ray photoelectron spectroscopy (ARXPS) [23]. *Yao* et al. synthesized a novel fluoroalkyl side-chain diblock copolymer, poly(3-hexylthiophene)-block-poly[3-(4-(3,3,4,4,5,5,6,6,7,7,8,8,8-tridecafluorooctyloxy)phenyl)-decyloxy]thiophene] (P3HT-b-P3FAT), successfully. And the fluorinated P3FAT polymer chains could aggregate on the surface of poly-(3-hexylthiophene) (P3HT) spontaneously during spin coating processes, driven by the low surface energy of fluoroalkyl side chains [24]. *Wei* et al. applied a fullerene derivative with a fluorocarbon chain in bulk-heterojunction polymer solar cells. It could migrate to the

surface of the organic layer during spin-casting owing to the low surface energy of the fluorocarbon, and form a very thin buffer layer between the polymer and the metal electrode by one step [25]. Nevertheless, as so far, there are few reports about fabricating organic active layer and cathode buffer layer based on the self-assembly of inorganic nanoparticles (such as ZnO NPs) simultaneously through a single step.

In this work, ZnO NPs were modified with triethoxy-1H,1H,2H,2H-tridecafluoro-n-octylsilane (TTFO), resulting in functionalized ZnOF NPs with surface segregation function of the fluoroalkyl chains. During the solvent annealing and thermal annealing process for the polymer solar cells, the low surface energy of the fluorocarbon could drive ZnOF NPs to migrate to the surface of organic layer to form a cathode buffer layer (CBL). Thus, both the active layer and CBL can be fabricated in a single step, which not only simplifies fabrication process and reduces the manufacturing cost of solar cells, but also increases the stability of the device, because the vertical phase separation in polymer photovoltaic devices is spontaneous and stable in thermodynamics. On the other hand, the movement of ZnOF NPs may actuate the polymer chains to stack more orderly, consequently forming favorable heterojunction morphology of active layer with remarkable phase separation, which is beneficial for boosting the power conversion efficiency (PCE) of polymer solar cells. The addition amount of ZnOF NPs and the degree of ZnOF NPs migration regulated by the film-formation process upon annealing in different solvents, produce obvious effects on the stacking of P3HT chains, the heterojunction (BHJ) morphology and the photovoltaic performance. After optimize the self-assembly CBL with 5 wt.% ZnOF NPs and annealing in good solvent of o-DCB, the PCE of the devices based on P3HT:PCBM active layer

enhances to 2.4% with open-circuit voltage (V_{oc}) of 0.49 V, short-circuit current density (J_{sc}) of 8.1 mA/cm² and fill factor (FF) of 61%, with comparison to the PCE of 1.2% for the device without any CBL.

Experimental Section

Materials

The poly(3-hexylthiophene) (P3HT, $M_w=48300$ g/mol, head-to-tail, regioregularity > 90%, Rieke Metals, Inc.), [6,6]-phenyl-C61-butyric acid methyl ester (PCBM, 99.5%; Nano-C) were used as received. ZnO NPs were synthesized following the process reported by *Beek* et al. [26]. The general procedure for the preparation of ZnO NPs as follows: 1.23 g of zinc acetate dihydrate ($Zn(CH_3COO)_2 \cdot 2H_2O$, 98%, AR, Aldrich) was dissolved in methanol (55 mL) at 60 °C under vigorous stirring. 25 mL potassium hydroxide (KOH) (90%, AR, Aldrich, 0.34 mmol mL⁻¹) solution in methanol was dropped into the $Zn(CH_3COO)_2 \cdot 2H_2O$ solution in 20 min under vigorous stirring. The reaction was held at 60 °C for additional 2 h to yield a homogeneous, clear and transparent solution, which contained ZnO NPs. After the ZnO NPs solution fell to room temperature, the triethoxy-1H,1H,2H,2H-tridecafluoro-n-octylsilane (TTFO) was added under vigorous stirring for 3 h to graft the functional groups of fluoroalkyl onto the ZnO NPs. Finally, let the solution alone to precipitate for another 2 h. In this report, the ZnO NPs grafting with functional fluoroalkyl chains were referred to as ZnOF NPs. Precipitate was separated by centrifugation and was washed three times with methanol. O-dichlorobenzene (o-DCB) was used to disperse ZnOF NPs, with the content of 20 mg/mL.

Fabrication of devices

Poly(3,4-ethylenedioxythiophene):poly(styrenesulfonate) (PEDOT:PSS) were prepared on indium tin oxide (ITO) substrates by spin coating. The conductive ITO substrates were cleaned in acetone, soap water, deionized water and isopropanol successively by ultrasonication and dried, treated with UV ozone for 20 min before spin coating PEDOT:PSS. Then, the substrates were annealed at 140 °C on a hot plate for 20 min. After that, P3HT:PCBM (1:1, w/w) blend or with (ZnO or ZnOF NPs) dissolved in o-DCB were spin-coated on the ITO/PEDOT:PSS substrates layer at 800 rpm for 40 s to form active layers. Upon solvent annealing, the films were placed in respective o-DCB and acetone vapor for 3 h. The additional cathode buffer layer was fabricated by spin-coating of ZnO or ZnOF NPs (20 mg/mL dissolved in methanol) above the active layer at 4000 rpm for 60 s. And then thermal annealed on a hot plate in glovebox at 150 °C for 10 min. At last, a 90 nm Al electrode was thermally deposited in vacuum (3×10^{-6} torr) when the film cooled down to room temperature slowly.

Characterizations

Hydrogen nuclear magnetic resonance (^1H NMR) and Fourier transform infrared spectroscopy (FTIR) were used to testify the chemical structure of ZnOF NPs. ^1H NMR spectra were collected on a Bruker AV 400 NMR spectrometer with deuterated CDCl_3 as the solvent and with tetramethylsilane ($\delta=0$) as the internal standard. FTIR spectra were recorded in a manner of KBr tablet on a Shimadzu IRPrestige-21 FT-IR spectrophotometer. All FTIR spectra were collected under the room temperature over a scanning range of 400-4000 cm^{-1} . Field emission transmission electron microscopy (TEM) was used to observe the dispersibility of ZnO and ZnOF NPs employed on JEOL, JEM-2100F. Atomic force microscopic (AFM) images were measured on a

nanoscope III A (Digital Instruments) scanning probe microscope using the tapping mode. To gain insight on the photophysics and electronic properties of the pure ZnO and ZnOF NPs, UV-vis-NIR spectroscopy (performed by Perkin-Elmer Lambda 750 with integrating sphere) was utilized. Survey X-ray photoelectron spectroscopy (XPS) was applied as an effective measure to certify the content of C 1s, F 1s, Zn 2p and O 1s on the surface of P3HT:PCBM:ZnOF (5%) on ITO substrate which was annealing in different solvent vapors. Ultraviolet photoelectron spectroscopy (UPS) was used for testing the energy-level diagram of the related materials. Current-voltage ($J-V$) characteristics of all devices were processed by Keithley 2400 Source Meter to test this mixture layer applied into the photovoltaic devices with unencapsulated condition and measured in air under 100 mW/cm^2 simulated AM 1.5 G irradiation (Abet Solar Simulator Sun 2000). A photo mask with an area of 0.04 cm^2 was used to define the active area of the device irradiated by light.

Results and Discussion

Synthetic route of the modified ZnO NPs (henceforth referred to as ZnOF) and the fabrication process of the polymer solar cells with self-assembly ZnOF NPs as cathode buffer layer has been shown in **Scheme 1**. The functional fluoroalkyl chains were successfully grafted onto the surface of ZnO NPs by the reaction between silane coupling agent of triethoxy-1H,1H,2H,2H-tridecafluoro-n-octylsilane (TTFO) and the hydroxyl groups of ZnO NPs, which could be verified by Fourier transform infrared spectrometer (FTIR) and hydrogen nuclear magnetic resonance (^1H NMR) characterization. As shown in **Figure 1** of FTIR spectra for ZnO NPs, TTFO and functionalized ZnOF NPs, a broad band from 3000 cm^{-1} to 3500 cm^{-1} are ascribed to the dangling hydroxyl groups on the surface of ZnO and ZnOF NPs. For ZnOF NPs,

the bands at 1246 cm^{-1} , 1200 cm^{-1} and 745 cm^{-1} are attributable to the asymmetrical C-F stretching mode of $-\text{CF}_2-$ and $-\text{CF}_3$ groups. The band around 1122 cm^{-1} , 1140 cm^{-1} and 1020 cm^{-1} originates from the stretching mode of Si-O group. The band around 1170 cm^{-1} was the result of the stretching mode of C-O group. The appearance of new bands proves that the fluorinated substitution of ZnO NPs has been realized.

Figure 2 illustrates the ^1H NMR spectra of ZnO NPs, TTFO and ZnOF NPs. The peak at 1.55 ppm (proton **a**) is assigned to protons from the hydroxyl groups absorbing on the surface of ZnO NPs. The peak at 1.22 ppm (9H, proton **b**), 3.83 ppm (6H, proton **c**), 0.88 ppm (2H, proton **d**) and 2.15 ppm (2H, proton **e**) are ascribed to different CH_2 and CH_3 of TTFO. For ZnOF NPs, the appearance of new single-peak at 1.28 ppm (proton **f**) assigned to methyl groups has been observed. Meanwhile, the peaks at 1.22 ppm (**b**), 3.83 ppm (**e**) belonging to TTFO disappear, which demonstrates that the functional ZnOF NPs have been synthesized successfully.

Grafting the fluoroalkyl chains onto the surface of ZnO NPs effectively increased their dispersion, which could be testified by field emission transmission electron microscopy (TEM). The TEM images of ZnO NPs and ZnOF NPs with 4 mg/mL in *o*-DCB are shown in **Figure 3**. It can be seen that the dispersion of ZnOF NPs is much better than ZnO NPs. Bringing in fluoroalkyl chains can prevent ZnO NPs from aggregating. The high magnification transmission electron microscope (HRTEM) images reveal clear lattice fringes of ZnO and ZnOF NPs. The marked spacing for the lattice fringes of ZnO NPs is about 0.28 nm, agreeing well with the expected separations of (002) planes in wurtzite ZnO. For ZnOF NPs, the spacing of lattice fringes is about 0.28 nm, which displays almost no variation after grafting with

fluoroalkyl chains.

The modified ZnOF NPs as additives mixing with poly(3-hexylthiophene):[6,6]-phenyl-C₆₁-butyric acid methyl ester (P3HT:PCBM) blend applied in polymer solar cells has been investigated. Driven by the surface segregation of the fluoroalkyl chains due to their low surface energy, ZnOF NPs can migrate from the active layer based on P3HT:PCBM blend to the surface during annealing process and self-assemble as a cathode buffer layer (CBL). The process flow of the polymer solar cells is illustrated in **Scheme 1**, which realizes fabricating both active layer and CBL through a single step. ZnOF NPs upward migration would induce the stacking of P3HT polymer chains, consequently availing the formation of tailored heterojunction morphology of active layer. In addition, the addition amount of ZnOF NPs is a critical factor in the formation of a continuous and dense buffer layer by self-assembling, which creates an effective contact interface between the active layer and cathode electrode and helps to resist the current leakage.

To investigate the self-organized ability of polymer chains in the active layer after incorporation of ZnOF NPs, the UV-vis absorption spectra of P3HT:PCBM blended with different amount of ZnOF NPs have been measured and shown in **Figure 4a**, which displays red shift of the P3HT:PCBM absorption. The distinct shoulder peak corresponding to vibronic features at about 610 nm, 560 nm and 510 nm are related to the 0-0, 0-1 and 0-2 transitions to the vibronic modes of the excited electronic state [27,28]. The height of the peak strongly depends on the intensity of interchain π - π stacking of P3HT polymers [29]. From the enlarged view of partial in **Figure 4b**, the red shift and the raised intensity are more pronounced, which indicates that local ordering and crystallinity of P3HT improve after adding ZnOF NPs. Because ZnOF

NPs possessing many fluorine atoms with low surface energy tend to migrate to the surface of the active layer in the film-formation process, which influences the crystallization thermodynamic and kinetic parameters of P3HT [30]. When the weight percent of ZnOF NPs is below 5 wt.%, the self-assembling of ZnOF NPs is favourable for the stacking of P3HT chains, consequently improving the crystallinity. And the positive effect further increases when the addition amount of ZnOF NPs runs up. While the weight percent of ZnOF NPs reaches to 10%, the stacking of P3HT can be suppressed by the aggregation of residual ZnOF NPs within the active layer. More remarkable, there is also a red shift for 10 wt.% amount, compared to that of pure P3HT:PCBM blend. The addition of ZnOF NPs as “dilutants” can increase the extent of phase separation between donor and acceptor, as well as the crystallization of P3HT.

The atomic force microscopy (AFM) images of P3HT:PCBM blended with different content of ZnOF NPs without solvent annealing have been displayed in **Figure 5**. The blank P3HT:PCBM without ZnOF NPs exhibits a smooth surface morphology and a root mean square (RMS) of 2.64 nm. Adding ZnOF NPs (2.5 wt.%) into the P3HT:PCBM blend, the RMS increases to 3.75 nm. From the UV-vis absorption spectra (**Figure 4**), we have presumed that the ZnOF NPs addition can increase the phase separation between donor and acceptor and the crystallization of P3HT, so the RMS growing is reasonable [31]. On the other hand, this may result from the small quantity of ZnOF NPs could not self-assemble as a continuous and dense layer on the surface, but rather only isolated nanoclusters. When the weight percent of ZnOF NPs raises from 2.5% to 5%, the RMS reduces to the minimum value (1.05 nm), owing to the formation of a favorable morphology after self-assembling of ZnOF NPs with

appropriate amount. However, the excess ZnOF NPs (10 wt.%) not only self-assemble as a complete buffer layer, but also remain partly within the active layer, which impairs the crystallinity of P3HT. Compared to P3HT:PCBM blended with ZnOF NPs (5 wt.%), the addition of ZnOF NPs (10 wt.%) results in a more rough morphology (RMS of 1.86 nm) and a relative blue shift of the UV-vis absorption related to P3HT:PCBM (**Figure 4**). It is noteworthy that the addition of ZnOF NPs is in favor of the stacking of P3HT chains, which agrees well with the obvious red shift of UV-vis absorption. Furthermore, the amount of ZnOF NPs has influence on the degree of crystallinity of P3HT to some extent. However, excessive ZnOF NPs remain partly within the active layer, which provide bridges for the cross-linking of PCBM, rather than the nucleating agent attributed to the hydrophilic characteristics [32], resulting in apparent aggregation of PCBM. On the other hand, it may hinder the segmental chains motion of P3HT, ultimately leading to a relatively poor ordering [33].

The ZnOF NPs with fluoroalkyl chains have undergone a gradual evolution from blending with P3HT:PCBM to self-assembling as an surface segregated monolayer (SSM), during which the migration degree of ZnOF NPs may have an a direct relationship with the stacking of P3HT chains. Therefore, adjusting the dynamic self-assembly process of ZnOF NPs by regulating the film-formation procedure could be an effective approach. During the film-forming, the optimized thermodynamic and kinetic parameters, such as polymer state in solution, solvent vapor pressure, and solubility of solutes [34,35] have contributed to the migrating of ZnOF NPs, consequently enhance the stacking of P3HT and the aggregation of fullerenes. Solvent annealing treatment can prolong the film-forming process and provide adequate time for polymer chains and ZnOF NPs to self-organize [36], which attributes to the solvent vapor penetrating into the film and increasing the space between the polymer

chains. At the same time, the migrating of ZnOF NPs gives P3HT chains an extra-stress, which is beneficial to forming oriented structures and enhancing the crystallinity [37].

In order to explore the relationship between film-formation process and migration extent of ZnOF NPs, the self-assembly of P3HT:PCBM blend containing ZnOF NPs (5 wt.%) without annealing or annealing in acetone and o-DCB vapor, respectively, were investigated. And the corresponding surface coverage of C 1s, F 1s, Zn 2p and O 1s elements has been measured by X-ray photoelectron spectra (XPS), as shown in **Figure 6**. The coverage of F 1s has positive correlation with the content of ZnOF NPs. The highest and the lowest coverage of F 1s have been observed for the blend system upon post-annealing in o-DCB and acetone, respectively. This may result from the difference between the solubility of P3HT in solvents. Upon post-annealing, o-DCB as a good solvent assists in P3HT chains stretching, consequently providing plenty space for the floating movement of ZnOF NPs to the surface [38]. As a consequence, surface segregated monolayer displays the highest coverage of F 1s. Meanwhile, P3HT chains self-organizing into ordered structure driven by the unobstructed migration of ZnOF NPs, agrees well the strongest intensity and largest red shift of the absorption peak associated with P3HT:PCBM (**Figure 7**), which will be described in detail later. However acetone as poor solvent upon post-annealing renders polymer chains to accumulate and form crystalline aggregates, which reduces the channels for ZnOF NPs migrating to the surface, consequently showing the lowest surface coverage of F1s.

In order to certify this hypothesis further, comparative experiments based on P3HT:PCBM blend mixed with ZnO and ZnOF NPs, as well as the blank system

(without adding any nanoparticles), were carried out. And the corresponding UV-vis absorption spectra (in **Figure 7**) without annealing or upon annealing in different solvents were measured. Compared to the blank system of P3HT:PCBM blend without solvent annealing, the red shift and raised intensity of the absorption peak related to P3HT:PCBM blend upon annealing in *o*-DCB is pronounced, which indicates that good solvent annealing optimization improves the local ordering and crystallinity of P3HT. For P3HT:PCBM blend upon annealing in acetone, the absorption peak displays apparent blue shift and decreased intensity, due to acetone as poor solvent upon post-annealing renders P3HT chains to accumulate and form crystalline aggregates which is unbeneficial for the formation of ordered structure. Furthermore, the absorption peaks of P3HT:PCBM blend mixed with ZnO NPs (5 wt.%) without annealing or annealing in *o*-DCB and acetone all exhibit the consistent blue shift compared to the pure P3HT:PCBM, owing to the existence of ZnO NPs aggregation may hinder the ordered stacking of P3HT. After adding self-assembly ZnOF NPs with excellent dispersibility upon the same annealing process, there are apparent red shifts of absorption peaks with comparison to the blank system. Because the migration of ZnOF NPs arising from the surface segregation of the fluoroalkyl chains gives P3HT chains extra-stress to form oriented structure and enhance the crystallization capacity [37]. But the incorporation of pristine ZnO NPs, the extra-stress does not exist. Therefore, it can be concluded that the migration of ZnOF NPs attributing to the surface segregation of the fluoroalkyl chains possesses obvious effects on the ordered stacking of P3HT chains.

The morphology of pure P3HT:PCBM and P3HT:PCBM blend mixed ZnOF NPs (5 wt.%) without annealing or upon annealing in different solvent vapor were measured

by AFM, and the corresponding height images are shown in **Figure 8**. For pure P3HT:PCBM, acetone as poor solvent upon post-annealing rendering polymer chains to aggregate results in a more rough morphology with RMS of 4.02 nm, compared to that without annealing (RMS of 2.64 nm). Upon annealing in good solvent of o-DCB, there is more remarkable phase separation between donor and acceptor, because o-DCB helps P3HT chains to stack and PCBM to aggregate to some extent. Thus the RMS increases to 4.28 nm. Incorporation of ZnOF NPs (5 wt.%) to the P3HT:PCBM blend, the RMS values change to 1.05 nm, 2.77 nm and 3.04 nm without annealing, with annealing in acetone and o-DCB, respectively. It can be illustrated that the self-assembly of ZnOF NPs as surface segregated CBL with more smooth morphology than that of pure P3HT:PCBM without any buffer layer. In combination with the former UV-vis results, it can be concluded that the existence of functionalized ZnOF NPs assist the stacking of donor polymer chains to form favorable morphology of active layer with remarkable phase separation, especially upon annealing optimization in o-DCB solvent.

The self-assembly ZnOF NPs as CBL applied in the polymer solar cells has been carried out. And the pristine and fluoroalkyl modified ZnO NPs spin-coated above the active layer as additional CBL have also been studied for comparison. The corresponding ultraviolet photoelectron spectroscopy (UPS) spectra and bandgaps of ZnO and ZnOF NPs have been measured, as shown in **Figure 9**. From the calculated energy levels data in **Table 1**, there are unobvious changes in the lowest unoccupied molecular orbital (LUMO) levels for ZnO and ZnOF NPs. The little variation of LUMO from -4.4 eV to -4.2 eV may not have direct effect on the electron transport, but it matches well with the energy level of PCBM and Ag electrode, which is in favor of the electron extraction. The *J-V* characteristics of devices based on different

cathode buffer layers forming by surface segregation of fluoroalkyl modified ZnO or additional spin-coating pristine and fluoroalkyl modified ZnO NPs above the active layer (in **Figure 9**) and the corresponding photovoltaic parameters, including open circuit voltage (V_{oc}), short-circuit current density (J_{sc}), fill factor (FF) and power conversion efficiency (PCE) (in **Table 2**) have been described. For the devices based on the additional CBL of ZnO and ZnOF NPs, the PCE are 2.0% and 2.2%, respectively. For pure P3HT:PCBM active layer without annealing, the absence of CBL results in low J_{sc} and FF, consequently with inferior PCE (only 1.2%). Incorporation of appropriate ZnOF NPs self-assembling as CBL optimizes the heterojunction morphology of the active layer, which is better for the enhancement of J_{sc} and FF. Upon annealing in good solvent of o-DCB, the stacking of donor P3HT chains helps to form the most favorable morphology of active layer with remarkable phase separation, achieving the best PCE of 2.4% with V_{oc} of 0.49 V, J_{sc} of 8.1 mA/cm² and FF of 61.1%. It is noticed that the photovoltaic performance of the device with a self-assemble CBL all display relatively low voltage and high photocurrent, with comparison to the devices with additional CBL. The low voltage results from the residue of additive ZnOF in the active layer (P3HT:PCBM blend), which can change the built-in potential. This conclusion agrees well with the study by Ning et al. [39]. According to the conduction band of ZnO NPs is -4.4 eV and that of ZnOF NPs is -4.2 eV (**Table 1**), it indicates that ZnOF should provide higher V_{oc} and built in potential than the non-functionalized ZnO NPs. However, the opposite tendency is observed, which appears that residual ZnOF in the active layer is acting as a recombination site affecting the transport properties of the system and reducing the V_{oc} of the device. A comprehensive effect of the built in voltage, work-function and active layer composition on V_{oc} has been described previously by Garcia-Belmonte

[40,41]. The high photocurrent comes from the order stacking of donor P3HT chains and the formation of a self-assemble thin and complete CBL. A thick CBL may decrease photocurrent, which has been reported by Mbule et al. [42]. Therefore, this novel approach could realize fabricating both active layer and CBL through a single step, which not only simplifies the fabrication procedure and reduces the manufacturing cost of the polymer solar cells, but also increases PCE by reduction of a Schottky barrier at the interface.

Conclusions

The spontaneous self-assembly of ZnOF NPs as the surface-segregated cathode buffer layer driven by the low surface energy of fluoroalkyl chains was present in the polymer solar cells based on P3HT:PCBM as active layer. The addition amount of ZnOF NPs and the migration degree regulated by the film-formation process upon annealing in different solvents, produce obvious effects on the stacking of P3HT chains, the heterojunction morphology and the photovoltaic performance. Small quantity of ZnOF NPs could not self-assemble as a continuous and dense layer on the surface, but rather only isolated nanoclusters. Excess ZnOF NPs (up to 10 wt.%) might suppress the stacking of P3HT due to the aggregation of residual ZnOF NPs within the active layer. The addition of appropriate functionalized ZnOF NPs assists the stacking of P3HT chains to form favorable heterojunction morphology of active layer with remarkable phase separation, which has been confirmed by the obvious red shift and raised intensity of the absorption peak related to P3HT:PCBM, as well as the RMS variation from AFM characterization. Upon post-annealing, o-DCB as a good solvent helps P3HT chains to stretch, consequently providing plenty space for the segregation movement of ZnOF NPs to the surface. Meanwhile, P3HT chains could

self-organize into ordered structure driven by the unobstructed migration of ZnOF NPs. However acetone as poor solvent upon post-annealing renders polymer chains to accumulate and form crystalline aggregates, which reduces the channels for ZnOF NPs migrating to the surface. After optimization of the addition amount of ZnOF NPs and annealing in good solvent of o-DCB, the PCE of the devices based on P3HT:PCBM active layer enhances to 2.4% with open-circuit voltage (V_{oc}) of 0.49 V, short-circuit current density (J_{sc}) of 8.1 mA/cm² and fill factor (FF) of 61%, with comparison to the PCE of 1.2% for the device without any CBL.

Acknowledgements

The financial supports for this work are provided by the National Natural Science Foundation of China (51273088 and 51302130), National Science Fund for Distinguished Young Scholars (51425304), National Basic Research Program of China (973 Program 2014CB260409), and Doctoral Programs Foundation of Ministry of Education of China (Grants 20133601120006). Zhijuan He and Licheng Tan contributed equally to this work.

References

1. Z.G. Zhang, J. Wang, Structures and properties of conjugated Donor-Acceptor copolymers for solar cell applications, *J. Mater. Chem.* 22 (2012), 4178-4187.
2. F. Zhang, M. Ceder, O. Inganäs, Enhancing the photovoltage of polymer solar cells by using a modified cathode, *Adv. Mater.* 19 (2007), 1835-1838.
3. N.S. Kang, B.K. Ju, T.W. Lee, D.H. Choi, J.M. Hong, J.W. Yu, Organic photovoltaic devices with a crosslinkable polymer interlayer, *Sol. Energy Mater. Sol. Cells* 95 (2011), 2831-2836.
4. H.L. Yip, S.K. Hau, N.S. Baek, H.J. Ma, K.Y. Alex, Polymer solar cells that use self-assembled-monolayer-modified ZnO/metals as cathodes, *Adv. Mater.* 20 (2008), 2376-2382.
5. Y. Zhang, K. Tajima, K. Hashimoto, Nanostructure formation in poly(3-hexylthiophene-block-3-(2-ethylhexyl)thiophene)s, *Macromolecules* 42 (2009), 7008-7015.
6. Y.E. Ha, M.Y. Jo, J. Park, Y.C. Kang, S.J. Moon, J.H. Kim, Effect of self-assembled monolayer treated ZnO as an electron transporting layer on the photovoltaic properties of inverted type polymer solar cells, *Synth. Met.* 187 (2014), 113-117.
7. A.F. Eftaiha, J.P. Sun, I.G. Hill, G.C. Welch, Recent advances of non-fullerene, small molecular acceptors for solution processed bulk heterojunction solar cells, *J. Mater. Chem. A* 2 (2014), 1201-1213.
8. G. Li, V. Shrotriya, J.S. Huang, Y. Yao, T. Moriarty, K. Emery, Y. Yang, High-efficiency solution processable polymer photovoltaic cells by self-organization of polymer blends, *Nat. Mater.* 4 (2005), 864-868.
9. M.T. Dang, L. Hirsch, G. Wantz, J.D. Wuest, Controlling the morphology and performance of bulk heterojunctions in solar cells. Lessons learned from the

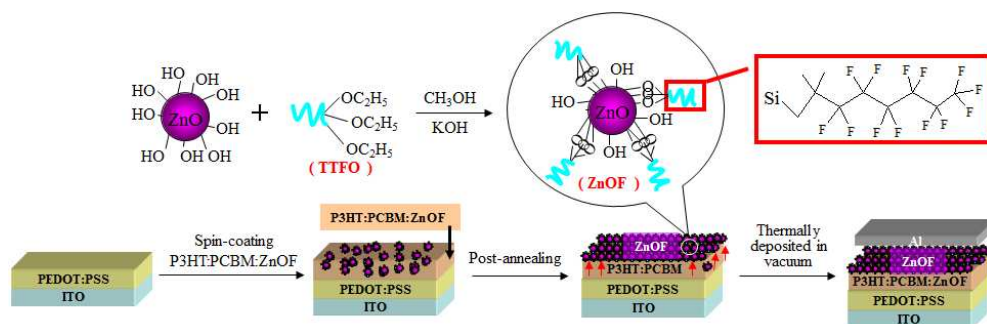
- benchmark poly(3-hexylthiophene):[6,6]-phenyl-C61-butyric acid methyl ester system, *Chem. Rev.* 113 (2013), 3734-3765.
10. Y. Geng, Q. Wei, K. Hashimoto, K. Tajima, Dipole layer formation by surface segregation of regioregular poly(3-alkylthiophene) with alternating alkyl/semifluoroalkyl side chains, *Chem. Mater.* 23 (2011), 4257-4263.
 11. Y.F. Zhang, R.Y. Liu, S.T. Lee, B.Q. Sun, The role of a LiF layer on the performance of poly(3,4-ethylenedioxythiophene):poly(styrenesulfonate)/Si organic-inorganic hybrid solar cells, *Appl. Phys. Lett.* 8 (2014), 083514.
 12. M.F. Xu, Y.J. Liao, F.S. Zu, J. Liang, D.X. Yuan, Z.K. Wang, L.S. Liao, Work-function tuneable and aqueous solution-processed Cs₂CO₃ for high-performance polymer solar cells, *J. Mater. Chem. A* 2 (2014), 9400-9404.
 13. Y.C. Yeh, S.S. Li, C.C. Wu, T.W. Shao, P.C. Kuo, C.W. Chen, Stoichiometric dependence of TiO_x as a cathode modifier on band alignment of polymer solar cells, *Sol. Energy Mater. Sol. Cells* 125 (2014), 125, 233-238.
 14. P.S. Mbule, T.H. Kim, B.S. Kim, H.C. Swart, O.M. Ntwaeaborwa, Effects of particle morphology of ZnO buffer layer on the performance of organic solar cell devices, *Sol. Energy Mater. Sol. Cells* 112 (2013), 6-12.
 15. D. Kim, J. Yoon, H. Kim, Selective area atomic layer deposited ZnO nanodot on self-assembled monolayer pattern using a diblock copolymer nano-template, *J. Nanosci. Nanotechnol.* 12 (2012), 1483-1486.
 16. M.G. Helander, Z.B. Wang, L. Mordoukhovski, Z.H. Lu, Comparison of Alq₃/alkali-metal fluoride/Al cathodes for organic electroluminescent devices, *J. Appl. Phys.* 104 (2008), 094510.
 17. C.Y. Neo, J.Y. Ouyang, LiF doped mesoporous TiO₂ as the photoanode of highly efficient dye-sensitized solar cells, *J. Power Sources* 241 (2013), 647-653.

18. Y.F. Zhang, R.Y. Liu, S.T. Lee, B.Q. Sun, The role of a LiF layer on the performance of poly(3,4-ethylenedioxythiophene):poly(styrenesulfonate)/Si organic-inorganic hybrid solar cells, *Appl. Phys. Lett.* 53 (2014), DOI:10.1063/1.4866968.
19. X.C. Bao, L. Sun, W.F. Shen, C.P. Yang, W.C. Chen, R.Q. Yang, P.M. Amassian, Facile preparation of TiO_x film as an interface material for efficient inverted polymer solar cells, *J. Mater. Chem. A* 2 (2014), 1732-1737.
20. S.W. Lee, Stoichiometric dependence of TiO_x as a cathode modifier on band alignment of polymer solar cells, *Sol. Energy Mater. Sol. Cells* 125 (2014), 233-238.
21. F.C. Chen, S.C. Chien, Nanoscale functional interlayers formed through spontaneous vertical phase separation in polymer photovoltaic devices, *J. Mater. Chem.* 19 (2009), 6865-6869.
22. M. Fenoll, J. Shim, C. Fuentes-Hernandez, K.H. Sandhage, B. Kippelen, Roles of thermally-induced vertical phase segregation and crystallization on the photovoltaic performance of bulk heterojunction inverted polymer solar cells, *Energy Environ. Sci.* 4 (2011), 3456-3460.
23. M.D. Clark, M.L. Jespersen, R.J. Patel, B.J. Leever, Predicting vertical phase segregation in polymer-fullerene bulk heterojunction solar cells by free energy analysis, *ACS Appl. Mater. Interfaces* 5 (2013), 4799-4807.
24. K. Yao, L. Chen, X. Chen, Y.W. Chen, Self-organized hole transport layers based on polythiophene diblock copolymers for inverted organic solar cells with high efficiency, *Chem. Mater.* 25 (2013), 897-904.
25. Q.S. Wei, T. Nishizawa, K. Tajima, K. Hashimoto, Self-organized buffer layers in organic solar cells, *Adv. Mater.* 20 (2008), 2211-2216.

26. J.E. Beek, M.M. Wienk, M. Kemerink, X.N. Yang, R.A. Janssen, Hybrid zinc oxide conjugated polymer bulk heterojunction solar cells, *J. Phys. Chem. B* 109 (2005), 9505-9516.
27. S. Gartner, M. Christmann, S. Sankaran, H. Rohm, E.M. Prinz, F. Pentth, A. Putz, A. E. Tureli, B. Pentth, Eco-friendly fabrication of 4% efficient organic solar cells from surfactant-free P3HT:ICBA nanoparticle dispersions, *Adv. Mater.* 26 (2014), 6653-6657.
28. Y. Lin, Q. Wei, G. Qian, L. Yao, J.J. Watkins, Morphology control in TiO₂ nanorod/polythiophene composites for bulk heterojunction solar cells using hydrogen bonding, *Macromolecules* 45 (2012), 8665-8673.
29. D. Chirvase, J. Parisi, J.C. Hummelen, V. Dyakonov, Influence of nanomorphology on the photovoltaic action of polymer-fullerene composites, *Nanotechnology* 15 (2004), 1317-1323.
30. C.V. Hoven, X.D Dang, R.C. Coffin, J. Peet, T.Q. Nguyen, G.C. Bazan, Improved performance of polymer bulk heterojunction solar cells through the reduction of phase separation via solvent additives, *Adv. Mater.* 22 (2010), E63-E66.
31. W.L. Wang, H.B. Wu, C.Y. Yang, C. Luo, Y. Zhang, J.W. Chen, Y. Cao, High-efficiency polymer photovoltaic devices from regioregular-poly(3-hexylthiophene-2,5-diyl) and [6,6]-phenyl-C-61-butyric acid methyl ester processed with oleic acid surfactant, *Appl. Phys. Lett.* 90 (2007), 183512.
32. W. Ma, X. Wang, J. Zhang, Effect of MMT, SiO₂, CaCO₃, and PTFE nanoparticles on the morphology and crystallization of poly(vinylidene fluoride), *J. Polym. Sci., Part B: Polym. Phys.* 48 (2010), 2154-2164.

33. B. Lim, J. Jo, S.I. Na, J. Kim, S.S. Kim, D.Y. Kim, A morphology controller for high-efficiency bulk-heterojunction polymer solar cells. *J. Mater. Chem.* 20 (2010), 10919-10923.
34. Y. Yao, J.H. Hou, Z. Xu, G. Li, Y. Yang, Effect of solvent mixture on the nanoscale phase separation in polymer solar cells, *Adv. Funct. Mater.* 18 (2008), 1783-1789.
35. X. Yang, J. Loos, Toward high-performance polymer solar cells: the importance of morphology control, *Macromolecules* 40 (2007), 1353-1362.
36. C. Sinturel, M. Vayer, M. Morris, M. A.Hillmyer, Solvent vapor annealing of block polymer thin films, *Macromolecules* 46 (2013), 5399-5415.
37. W.R. Hwang, G.W.M. Peters, M.A. Hulsen, H.E.H. Meijer, Modeling of flow-induced crystallization of particle-filled polymers, *Macromolecule* 39 (2006), 8389-8398.
38. L.L. Chang, H.W.A. Lademann, J.B. Bonekamp, K. Meerholz, A.J. Moulé, Effect of trace solvent on the morphology of P3HT:PC₆₁BM bulk heterojunction solar cells, *Adv. Funct. Mater.* 21 (2011), 1779-1787.
39. Z.J. Ning, D. Zhitomirsky, V. Adinolfi, B. Sutherland, J. Xu, O. Voznyy, P. Maraghechi, X. Lan, S. Hoogland, Y. Ren, E. H.Sargent, Graded doping for enhanced colloidal quantum dot photovoltaics, *Adv. Mater.* 25 (2013), 1719-1723.
40. A. Guerrero, L.F. Marchesi, P.P. Boix, S. Ruiz-Raga, T. Ripolles-Sanchis, G. Garcia-Belmonte, J. Bisquert, How the charge-neutrality level of interface states controls energy level alignment in cathode contacts of organic bulk-heterojunction solar cells, *ACS Nano* 6 (2012), 3453-3460.
41. A. Guerrero, N.F. Montcada, J. Ajuria, I. Etxebarria, R. Pacios, G.

- Garcia-Belmonte, E. Palomares, Charge carrier transport and contact selectivity limit the operation of PTB7-based organic solar cells of varying active layer thickness, *J. Mater. Chem. A* 1 (2013), 12345-12354.
42. P.S. Mbule, T.H. Kim, B.S. Kim, H.C. Swart, O.M. Ntwaeaborwa, Effects of particle morphology of ZnO buffer layer on the performance of organic solar cell devices, *Sol. Energy Mater. Sol. Cells* 112 (2013), 6-12.



Scheme 1. Synthetic route of the functionalized ZnOF NPs and fabrication process of the polymer solar cells with self-assembly ZnOF NPs as cathode buffer layer.

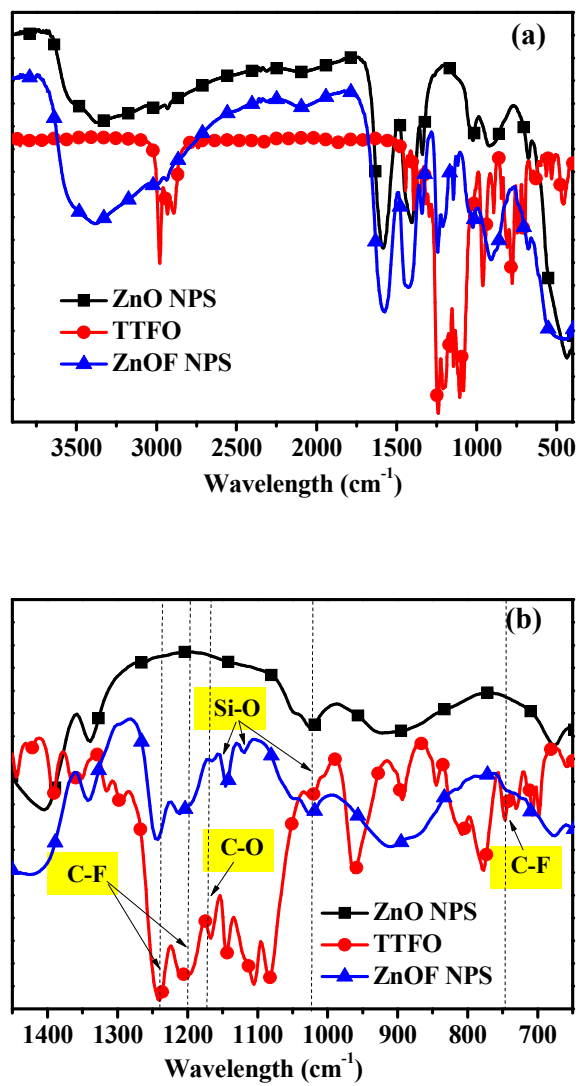


Figure 1. FTIR spectra of TTFO, bare ZnO and ZnOF NPs.

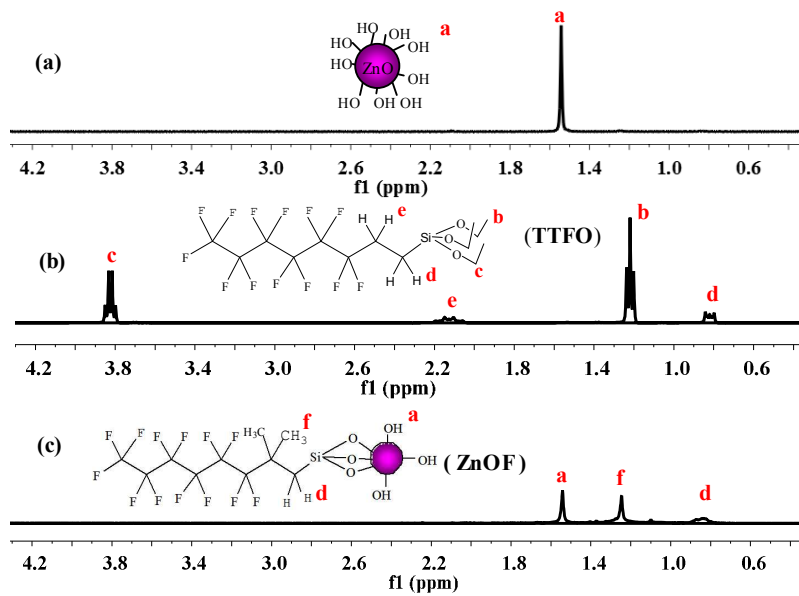


Figure 2. ^1H NMR (400 MHz, CDCl_3) of ZnO NPs, TTFO and ZnOF NPs.

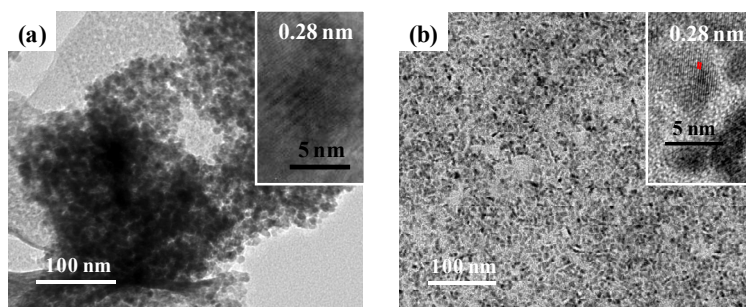


Figure 3. TEM images of (a) ZnO NPs and (b) ZnOF NPs, respectively. The insets show the corresponding high-resolution TEM images.

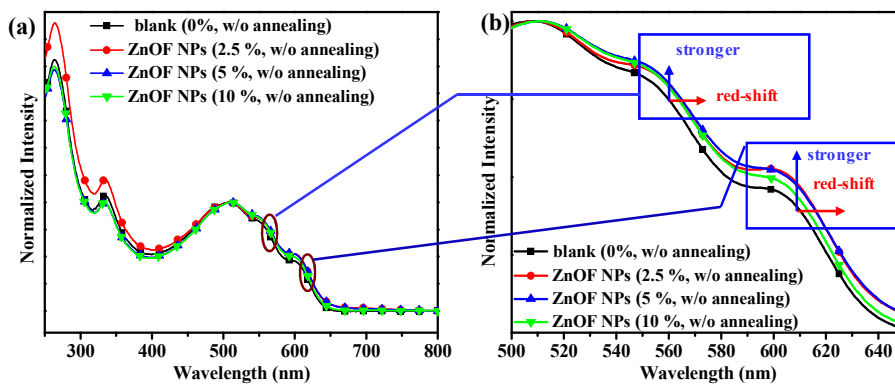


Figure 4. (a) Normalized absorbance spectra of P3HT:PCBM blend with different content of ZnOF NPs without solvent annealing and (b) the enlarged view of partial.

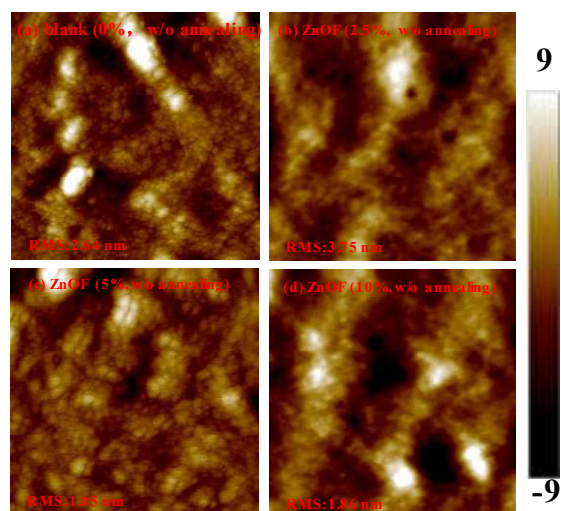


Figure 5. AFM height images of P3HT:PCBM blend with different content of ZnOF NPs without solvent annealing. The image sizes are all $3 \mu\text{m} \times 3 \mu\text{m}$.

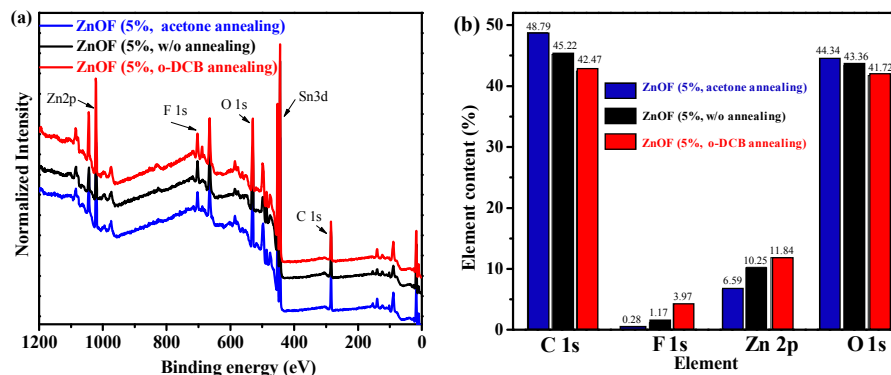


Figure 6. (a) Survey X-ray photoelectron spectra and (b) the coverage of C 1s, F 1s, Zn 2p and O 1s on the surface of P3HT:PCBM:ZnOF (5 wt.%) on ITO substrate.

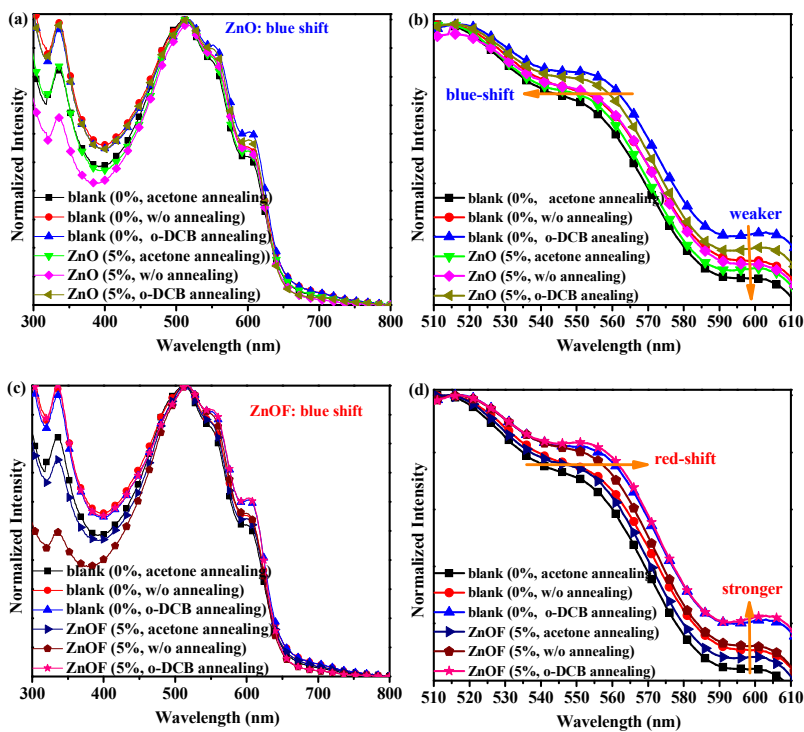


Figure 7. UV-vis normalized absorbance spectra of P3HT:PCBM blend film: (a) without or with ZnO NPs (5 wt.%), (c) without or with ZnOF NPs (5 wt.%), (b) and (d) the corresponding drawings of partial enlargement.

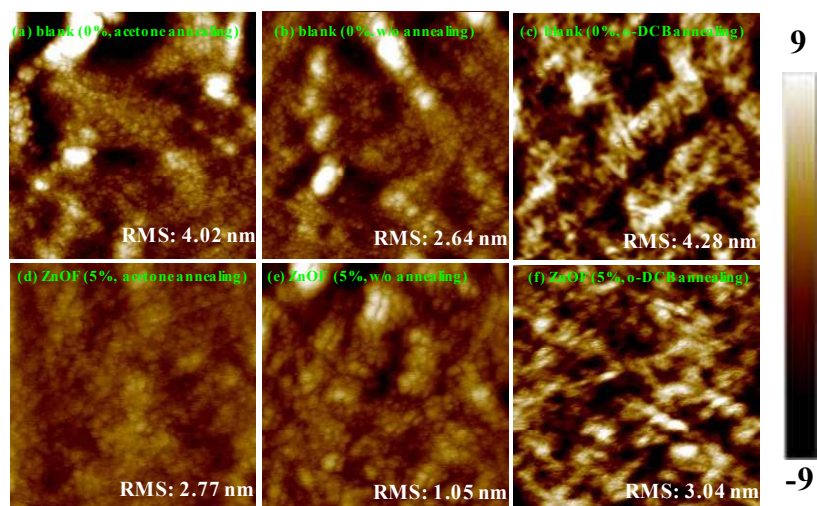


Figure 8. AFM height images of pure P3HT:PCBM and P3HT:PCBM blend mixed with ZnOF NPs (5 wt.%) without annealing or upon annealing in different solvent vapor. The image sizes were all $3 \mu\text{m} \times 3 \mu\text{m}$.

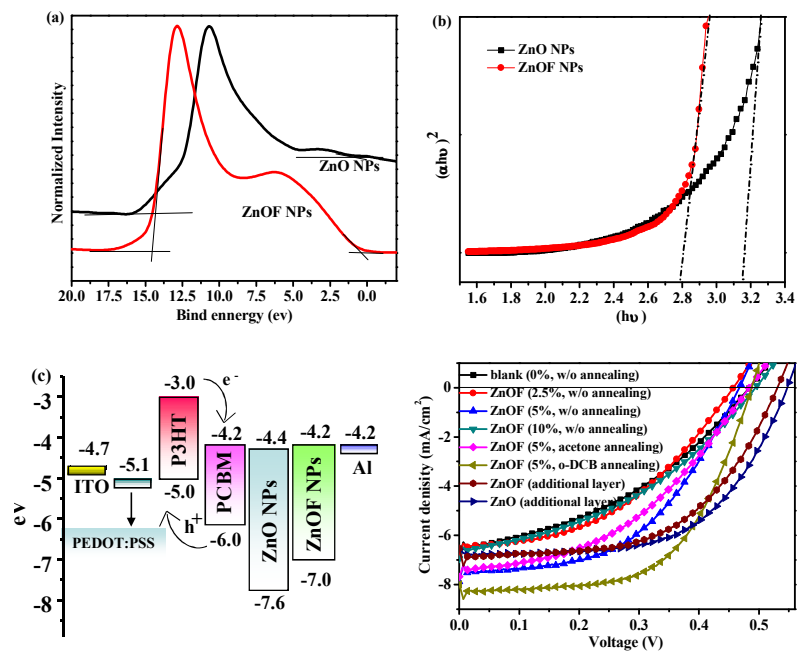


Figure 9. (a) Ultraviolet photoelectron spectroscopy (UPS) spectra of ZnO and ZnOF NPs, (b) the bandgaps of ZnO and ZnOF NPs, (c) energy-level diagram of the related materials used for device fabrication and (d) J - V characteristics of devices' structure:

ITO/PEDOT:PSS/P3HT:PCBM:(with or without adding ZnOF NPs)/Al and

ITO/PEDOT:PSS/P3HT:PCBM/additional (ZnOF or ZnO) layer/Al.

Table 1. Energy levels of ZnO and ZnOF NPs.

Samples	E_{cutoff} (eV) ^a	E_{onset} (eV) ^b	HOMO (eV) ^c	LUMO (eV) ^d
ZnO NPs	15.56	0.56	-7.6	-4.4
ZnOF NPs	14.58	0.36	-7.0	-4.2

^aThe high binding-energy cutoff. ^bThe onset relative to the Fermi level (E_F) of Au (at 0 eV), where the E_F was determined from the Au substrate. ^cCalculated according to $\text{HOMO} = h\nu - (E_{\text{cutoff}} - E_{\text{onset}})$, where $h\nu$ is the incident photon energy, $h\nu = 21.22$ eV. ^dCalculated from the HOMO level and optical band gap obtained from UV-vis absorption spectra.

Table 2. Photovoltaic performance of polymer solar cells based on different cathode buffer layers forming by surface segregation of fluoroalkyl modified ZnO or additional spin coating above active layer.

Different cathode buffer layers	J_{sc} (mA/cm ²)	V_{oc} (V)	FF (%)	PCE (%)
blank (w/o, w/o annealing)	6.4±0.7	0.46±0.03	38.5±1.9	1.2±0.0
ZnOF (2.5%, w/o annealing)	6.5±0.2	0.46±0.02	42.7±0.7	1.3±0.4
ZnOF (5%, w/o annealing)	7.9±0.0	0.47±0.01	48.0±3.3	1.8±0.1
ZnOF (10%, w/o annealing)	7.1±0.2	0.48±0.01	40.0±3.1	1.3±0.1
ZnOF (5%, acetone annealing)	7.5±0.2	0.49±0.01	43.7±1.1	1.6±0.1
ZnOF (5%, o-DCB annealing)	8.1±0.1	0.49±0.00	61.1±1.4	2.4±0.1
ZnOF (additional layer)	6.8±0.3	0.53±0.01	56.2±2.5	2.0±0.1
ZnO (additional layer)	6.7±0.3	0.55±0.01	59.2±1.9	2.2±0.1

All values represented averages from fifteen 0.04 cm² devices on a single chip. The structure of devices: ITO/PEDOT:PSS/P3HT:PCBM:(with or without adding ZnOF NPs)/Al and ITO/PEDOT:PSS/P3HT:PCBM/additional (ZnOF or ZnO) layer/Al.

Highlights

Formation of Cathode Buffer Layer by Surface Segregation of Fluoroalkyl

Modified ZnO for Polymer Solar Cells

Licheng Tan, Zhijuan He, Yiwang Chen*

Cathode buffer layer by surface segregation of fluoroalkyl modified ZnO was present in the polymer solar cells based on P3HT:PCBM.

Graphical abstract

